

SELECTED TOPICS ON HERA PHYSICS *

L. LABARGA

Universidad Autónoma de Madrid, Canto Blanco, Madrid34, Spain

(Received April 29, 1999)

In this talk I present some of the most relevant results obtained by the HERA experiments up to now.

PACS numbers: 12.38.-t, 12.38.Qk, 13.65.+i, 13.85.Hd

1. Introduction

I would like first to sketch the outline of the talk following a very basic introduction to HERA physics.

HERA collides 27 GeV positrons (e^+) with protons (p). The e^+ is believed to be an elementary particle whereas the p is known not to be elementary and it is believed to be formed by 3 valence u, u, d quarks inside a cloud of many interacting gluons and sea quarks. Therefore, if we assume that the above picture is correct, in HERA the e^+ is probing the p this allowing us to learn about the composition of the latter. This will be the topic of Section 3 where the measurement of the proton structure function, $F_2(x, Q^2)$, will be extensively discussed.

For the same reason, HERA also allows us to learn about the fundamental interactions, *i.e.* those between the particles believed to be elementary. First, we can learn about the interactions between the quarks and gluons within the proton from a study of the behavior of our measured $F_2(x, Q^2)$ (Section 3). Second, we will contrast with the data the definite predictions that the Electroweak (EW) theory has for the interactions between the incoming lepton and the partons within the proton (Section 4).

QCD predicts important corrections to the above processes. They will be contrasted in several analyses of multijet production (Section 5) and charm production (Section 6).

* Presented at the XXVII International Meeting on Fundamental Physics, Sierra Nevada, Granada, Spain, February 1-5, 1999.

But before starting with the physics program I would like to introduce briefly the kinematics at HERA and the experimental apparatus: the detectors H1 and ZEUS. Most of the results I will present in this talk are from the ZEUS experiment.

2. The HERA kinematics and experimental apparatus

At the Born level lepton–proton scattering is understood to proceed via the exchange of a virtual gauge boson which interacts with one of the partons within the proton (see Fig. 1-left).

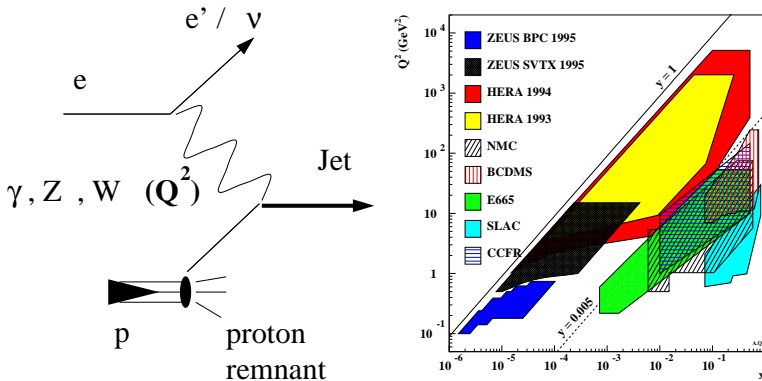


Fig. 1.

There are several variables which can be used to describe the kinematics of the reaction: Q^2 is the square of the four-momentum transferred at the lepton vertex (with a minus sign). x is the Bjorken variable; in the naive Quark Parton Model (QPM) it would be the fractional momentum of the proton carried out by the struck quark. y is the fractional energy transfer between the e^+ and the p in the p rest frame. W is the virtual boson–proton invariant mass; it is also the invariant mass of the final state hadronic system.

Once fixed the initial state, the kinematics of the reaction is fully determined with only two final state variables. Therefore, only two of the above (or others) are independent, the rest can be calculated out of them (see for example [1]).

Depending upon the electric charge of the exchanged boson we classify the reactions as Neutral Current (NC) or Charged Current (CC).

Depending on the virtuality of the exchanged boson, we consider two kinematical regimes: Deep Inelastic Scattering (DIS), when Q^2 is larger than a few GeV^2 or Photoproduction ($Q^2 \approx 0$). In the latter case, as the photon is almost real, the e^+p reaction can be viewed as a γp scattering.

The energies of the HERA beams allow for a kinematical coverage extending by far those from previous fixed-target experiments. The range in Q^2 , x , W covered by HERA is $0 \rightarrow 45000 \text{ GeV}^2$, $2 \cdot 10^{-6} \rightarrow 1$, $\rightarrow 300 \text{ GeV}$; *i.e.* approximately 2, 3, 1 orders of magnitude beyond previous experiments.

The HERA detectors measure both the scattered e^+ (its energy, $E_{e'}$, an scattering angle, $\theta_{e'}$) and the final state hadronic system (which we could characterize by its final energy E_H and angle θ_H , which, in the QPM would correspond with the scattering angle of the struck quark, see [1] for details). *I.e.* we measure 4 final state variables when only two of them are independent. We therefore have an over constrained system which will help us greatly in the study of the systematics of our measurements¹.

Respecting what we see in the detector, one important example is the relationship between the virtuality of the reaction and the scattered lepton variables, $Q^2 = 2E_e E_{e'}(1 - \cos \theta_{e'})$, where E_e is the e^+ beam energy. Other relationships can be found in [1]. From the previous equation we see that for low Q^2 the direction of the scattered e^+ will be very close to that of the incoming e^+ (*i.e.* it will escape down the beam pipe), whereas for large Q^2 the e^+ will be scattered off at large angles.

In the H1 NC candidate event display shown in Fig. 2-left we can see the key components of the H1 detector for these analyses, namely the tracking system and the calorimeter. The H1 calorimeter is of the liquid argon type with lead plates as passive material in the electromagnetic section and steel in the hadronic section. The H1 calorimeter is characterized by a very fine granularity and by an excellent energy resolution in the electromagnetic section ($\sigma(E)/E \simeq 12\%/\sqrt{E/\text{GeV}}$).

In contrast, the ZEUS calorimeter, which with the central tracker are the key components for the ZEUS analyses (see the ZEUS CC candidate event display shown in Fig. 2-right), is a uranium-scintillator sandwich type calorimeter with photomultiplier readout. It has a coverage of 99.7% of the solid angle and a superb hadronic energy resolution of $\simeq 35\%/\sqrt{E/\text{GeV}}$.

Last but not least both detectors measure the Luminosity delivered by HERA in the corresponding interaction regions by the rate of bremsstrahlung of high energy photons in the process $ep \rightarrow ep\gamma$ using lead-scintillator calorimeters located at approximately 100 meters downstream from their interaction points.

The calorimeters of both detectors measure the energy deposited in their different cells. As the spatial location of those cells are known, one can derive the corresponding 4-momentum for every cell. From those measurements and using complicated algorithms which are based on the pattern of energy deposition in the calorimeter one can identify the scattered positron to a

¹ Obviously this does not hold for CC reactions where we only measure the hadronic variables.

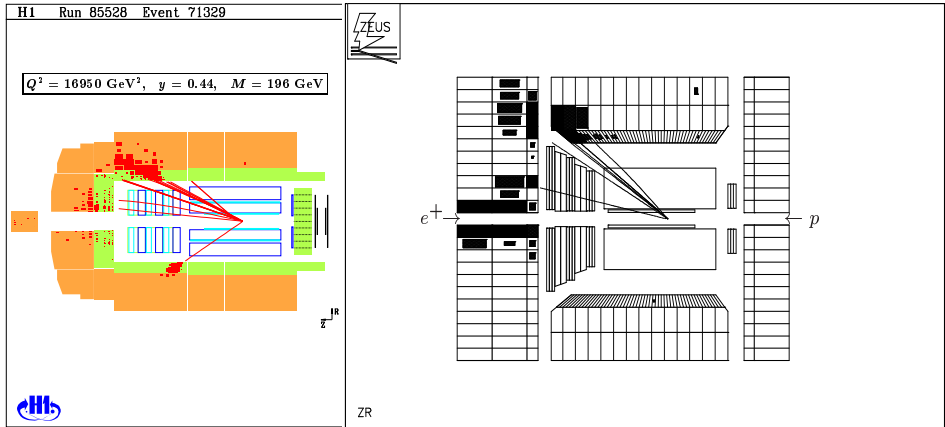


Fig. 2.

high degree of purity and reconstruct E'_e and θ'_e . The algorithms also use the information of the central tracker if available.

With the information from the calorimeter cells not assigned to the scattered positron one can measure several hadronic quantities like transverse momentum and in particular the energy and angle of the hadronic system (E_H , θ_H) mentioned previously.

3. The proton structure function $F_2(x, Q^2)$.

The double differential cross section for e^+p NC DIS can be factorized, on the basis of general considerations, into a $2 \rightarrow 2$ cross section and a (x, Q^2) dependent term which accounts for the proton having substructure. In the kinematical range where electro-weak corrections are negligible,

$$\frac{d^2\sigma}{dx dQ^2} = \frac{4\pi\alpha^2}{xQ^4} \left(\frac{y^2}{2} 2xF_1(x, Q^2) + (1-y)F_2(x, Q^2) \right). \quad (1)$$

In the QPM, *i.e.* with the proton consisting of non interacting partons, the two functions F_1 and F_2 scale, that is, they are independent of the 4-momentum transfer of the reaction and they are related between them and to the parton densities in the proton as $F_2(x) = 2xF_1(x) = \sum_i e_i^2 xq_i(x)$.

Due to gluon bremsstrahlung from the quark lines and gluon splitting, QCD introduces important modifications to this picture, the proton becoming a very complex cloud of quarks and self-interacting gluons. As a consequence, the above properties are broken. In particular scaling is broken and some logarithmic Q^2 dependence is expected in $F_2(x, Q^2)$. In addition the above relationship between $F_2(x)$ and $F_1(x)$ doesn't hold any more. In

QCD, $F_2(x, Q^2) - 2xF_1(x, Q^2) = F_L(x, Q^2) > 0$. However, the expected corrections are very small in the kinematical region mapped by our analysis ($F_L(x, Q^2)$ is only appreciable at large values of y). Also, perturbative QCD predicts that $F_2(x, Q^2)$ should grow faster than any power of $\ln(1/x)$ when x approaches 0 [2].

The proton structure function $F_2(x, Q^2)$ receives contributions from the valence quarks, the quarks from the sea and the gluons. These contributions are parametrized in terms of partonic densities: $q_V(x, Q^2)$, $q_S(x, Q^2)$ and $g(x, Q^2)$ respectively. The ultimate goal of any experiment would be to extract precise (x, Q^2) maps for these densities. This is difficult and, for the time being, only in particular reactions we can directly probe one of these types of densities (see, for example, later in this talk). Instead, what we do is to measure as precisely as feasible the (x, Q^2) map of F_2 , and from it, try to extract the different type of partonic distributions based on the QCD expectations for their behavior. Therefore we are doing two things at the same time: testing QCD and measuring the proton content.

As mentioned before, one relevant expectation from QCD is that F_2 should rise strongly when decreasing x for intermediate Q^2 . This rise comes from the corresponding rise of the gluon density which should have a functional x dependence as a power, $xg(x, Q^2) \sim x^{-\lambda}$, of a negative value close to 0.5 [3], $\lambda \approx (\alpha_s/\pi) \cdot 12 \ln 2 \approx 0.5$.

Finally and to complete the previous arguments I should recall that HERA is extending the x, Q^2 proton mapping by two orders of magnitude towards both low x and high Q^2 . This allows a detailed investigation of the above QCD predicted features.

The double differential cross section for e^+p NC DIS of Eq. 1 can be rewritten (in the region where EW corrections are negligible) as

$$\frac{d^2\sigma}{dx dQ^2} = \frac{2\pi\alpha^2}{xQ^4} (1 + (1-y)^2) F_2(x, Q^2) - y^2 F_L(x, Q^2). \quad (2)$$

The experimental procedure (see for example [5]) starts by counting the reconstructed number of NC DIS final states lying in the different (x, Q^2) bins. The obtained numbers are corrected for detector acceptances and smearing, and for QED initial state radiation. Dividing by the luminosity we arrive to $d^2\sigma/dxdQ^2_{\text{corr}}$. From it, $F_2(x, Q^2)$ is extracted by putting in F_L using the prescription by QCD (its contribution is at the 1% level).

For the estimation of the correction factors, Monte Carlo models have been used. They incorporate EW radiative corrections at first order, QCD corrections at LO+PS, fragmentation, our best knowledge of the proton's partonic density and a detailed detector simulation. Their description of the measured final states is excellent (see for example Fig. 5 in [5]).

Fig. 1-right shows the (x, Q^2) regions covered by the different $F_2(x, Q^2)$ measurements up to now, including those from fixed target experiments.

I am going to discuss first the results by ZEUS with the 1993 and 1994 HERA data [4, 5]. They cover Q^2 values from ≈ 2 up to ≈ 5000 GeV² with x extending down to almost 10^{-5} (see Fig. 1-right).

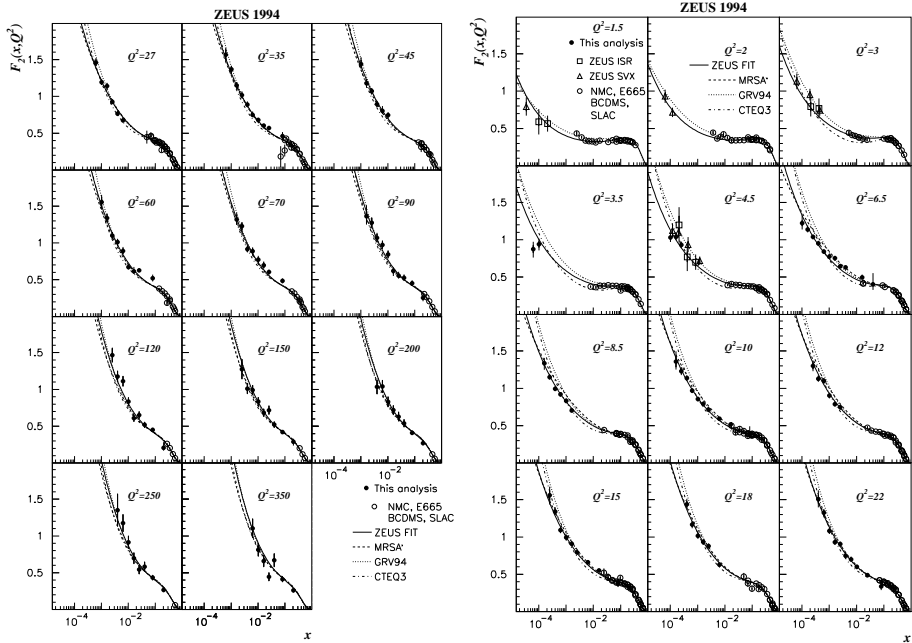


Fig. 3.

Fig. 3 shows the measured $F_2(x, Q^2)$ as a function of x for Q^2 intervals centered at values between 1.5 and 350 GeV². For the sake of brevity the corresponding results at higher Q^2 are not shown. For $27 < Q^2 < 350$ GeV² (Fig. 3-right), the QCD predicted raise of F_2 with decreasing x (down to 10^{-3}) is apparent. Results from fixed target experiments covering the high x region are also shown (for their references see [5]), they link well with the high x HERA data.

Both, fixed target and HERA results are well described by the QCD based parametrizations shown in Fig. 3. They are calculations by Martin, Roberts and Stirling (MRSA', [6]), by Glück, Reya and Vogt (GRV94, [7]) and by the CTEQ Collaboration (CTEQ3, [8]). They are based on the conventional NLO QCD evolution equations. They assume a certain shape of the x behavior at a starting Q_0^2 value and use the DGLAP [9] equations to get predictions at any Q^2 .

CTEQ3 and MRSA' assume an $x^{-\lambda}$ behavior when $x \rightarrow 0$, $Q_0^2 \approx 3 - 4 \text{ GeV}^2$ (the idea is to keep $Q_0^2 \gg \Lambda$, being their methods not valid for lower Q_0^2), and their parameters were determined from fits to fixed target and HERA-1993 ($Q^2 > 7 \text{ GeV}^2$) results.

In contrast, GRV assumes that all quark and gluon distributions have a valence like shape (*i.e.* vanish for $x \rightarrow 0$) at a very low $Q_0^2 = 0.34 \text{ GeV}^2$. By using DGLAP to evolve from Q_0^2 to any Q^2 , they predict that F_2 should rise towards low x even at very low $Q^2 \approx 1 \text{ GeV}^2$. The parameters in GRV were determined using only fixed target data (*i.e.* high x values). As a result, little freedom was left for further adjustment with HERA data.

The ZEUS 1994 lowest Q^2 results on F_2 are shown in Fig. 3-right. The Q^2 range covered is from 22 GeV^2 down to 1.5 GeV^2 . The lowest x value reached is $\approx 5 \times 10^{-5}$. Even at the lowest Q^2 interval F_2 is still rising with decreasing x , although less strongly than at higher Q^2 . The MRSA' and CTEQ3 parametrizations give a reasonable description of the data in the Q^2 range where they are supposed to be valid. GRV94 is able to provide a reasonable description of the data even at the lowest Q^2 bin, in which the data shows the raise predicted by them. From this analysis it seems that the low Q^2 limit down to which perturbative QCD is able to describe the data is indeed very low.

But there is experimental evidence for such a limit: at a given Q^2 the raise of F_2 with decreasing x is equivalent to the corresponding raise of the total γp cross section ($\sigma_{\text{tot}}^{\gamma^* p}$) with W . On the other hand, at very low Q^2 ($Q^2 \approx 0$) the raise of $\sigma_{\text{tot}}^{\gamma^* p}$ with W is measured to be very small and consistent with the corresponding behavior of σ_{tot}^{pp} , being both ($\sigma_{\text{tot}}^{\gamma^* p}$ and σ_{tot}^{pp}) well described in terms of the Regge theory by the model of Donachie and Landshoff [10]. Therefore there must be a low Q^2 value, not much lower than the range covered by the HERA 94 data, at which a "transition region" occurs in which F_2 flattens down and reaches the Regge behavior.

To study these important issues, the two HERA experiments revised slightly their physics program and built little ad-hoc detectors to investigate the very low Q^2 region. ZEUS built two beam pipe electromagnetic calorimeter modules and placed them on two sides of the beam pipe at 2937 mm from the interaction point in the rear (positron) direction. With this subdetector (named Beam Pipe Calorimeter, BPC), ZEUS could measure e^+ scattered off at very small scattering angles (see Sec. 2) and extract F_2 in the very low Q^2 range $0.11 \leq Q^2 \leq 0.65 \text{ GeV}^2$ [11] (see Fig. 1-right).

In addition, and in order to fill the gap in Q^2 between the BPC data and the HERA 1994 results, a dedicated HERA run with the collision point shifted 700 mm w.r.t. nominal in the proton direction was carried out (SVTX or SVX). In this case, the main calorimeter could itself measure very low scattering angles. The Q^2 range covered was $0.6 \leq Q^2 \leq 17 \text{ GeV}^2$ [12] (see Fig. 1-right).

ZEUS 1995

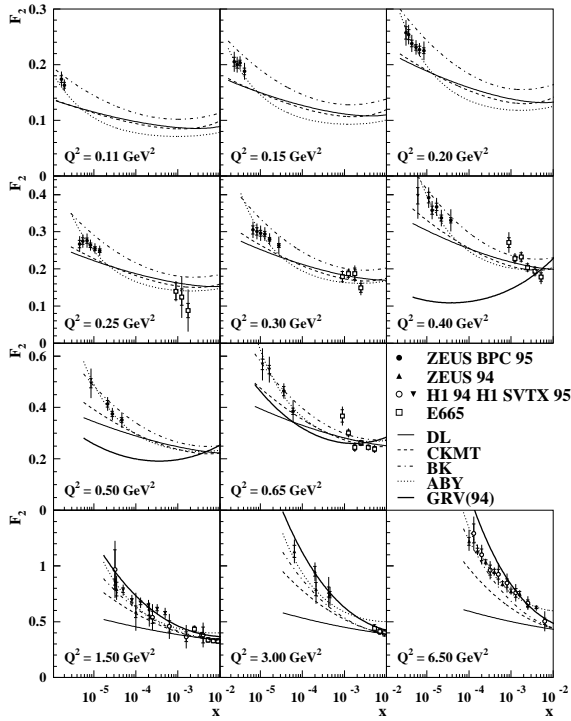
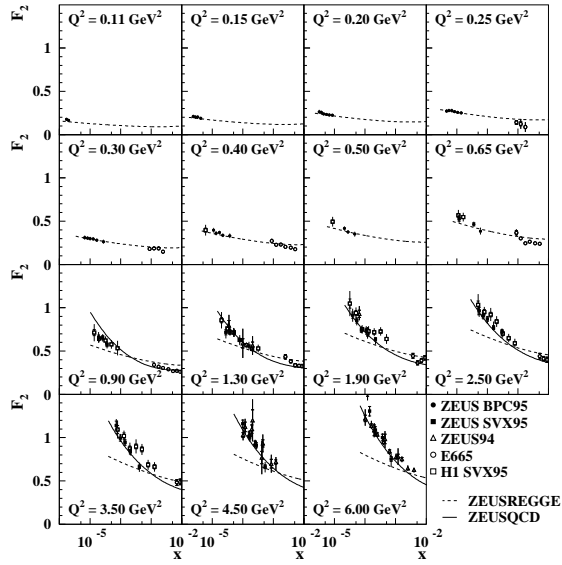


Fig. 4.

The results are shown in Fig. 4 where the vertical scale for the different Q^2 intervals is either kept constant for a good overview of the behavior of F_2 with Q^2 (Fig. 4-up) or it has been enlarged properly to allow a detailed comparison with models (Fig. 4-down). Results from fixed target experiments have been included in Fig. 4 when available.

It is apparent in Fig. 4-up how the strong x dependence observed at the higher Q^2 intervals flattens out when decreasing Q^2 and reaches the Regge behavior at $Q^2 \approx 0.5 \text{ GeV}^2$. Looking now to Fig. 4-down we see how GRV94 gives a reasonable description of the data for Q^2 values down to $\approx 1.5 \text{ GeV}^2$ but fails more and more when further decreasing Q^2 . On the contrary, the Regge based model by Donachie and Landshoff (DL) which fails at high Q^2 , approaches reasonably well the data at the lowest Q^2 intervals. It seems therefore that the transition between the perturbative QCD and the soft photoproduction regime occurs at around $Q^2 \approx 0.5 \text{ GeV}^2$.

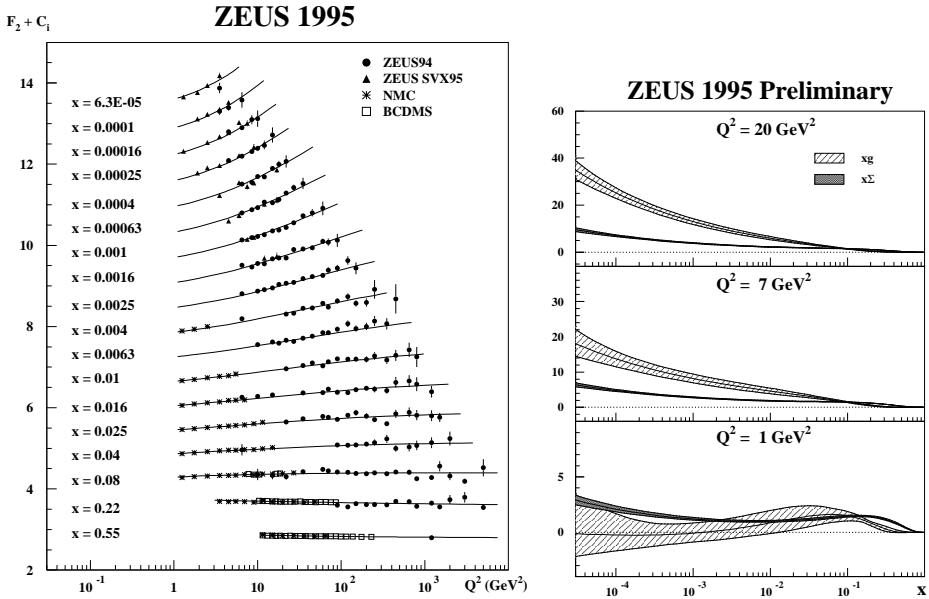


Fig. 5.

To finalize this discussion I find worth mentioning that the NLO QCD calculation by Adel, Barreiro and Ynduráin (ABY, [13]), featuring a somehow saturating α_s , is able to describe the low x data along the whole Q^2 range covered.

I now turn to a quick study on the QCD-expected scaling violation in the F_2 data. Fig. 5-left shows the 1994 and shifted vertex ZEUS $F_2(x, Q^2)$ data as a function of Q^2 for different x ranges. Results from fixed target

experiments are also shown. Clear scaling violations are apparent. They become stronger with decreasing x as predicted by QCD. The line is the result of a NLO QCD fit by ZEUS (see [5]). From this fit we can extract the gluon density within the proton. The result is shown in Fig. 5-right for three different Q^2 intervals centered at 20, 7 and 1 GeV² respectively. The gluon density (xg) is small at low Q^2 but raises rapidly (at low x) with increasing Q^2 .

4. Study of electroweak reactions

HERA, in addition of being a unique facility for probing the proton down to very small distances, allows stringent test of the electroweak theory in a kinematical regime complementary to that offered by the LEP collider. The first important result by HERA in this context was the first experimental observation of the effects of the W^\pm propagator [14]. HERA is also a unique facility to search for s-channel resonant production of new particles possessing coupling to lepton-quark pairs with masses up to $M \approx 300$ GeV. In this talk I will not go through the different particle searches carried out by the HERA Collaborations, instead I will concentrate in what is its complementary, namely the accord or disagreement of the Standard Model (SM) predictions with the measured production cross sections in a kinematic region corresponding to the largest values of the achievable M 's (*i.e.* very large Q^2 and/or very large values of x).

In this kinematic regime the Standard Model Born cross section for the DIS NC (Eq. 1) has to be generalized to account properly for electroweak effects

$$\frac{d^2\sigma}{dx dQ^2} = \frac{2\pi\alpha^2}{xQ^4} [Y_+ \mathcal{F}_2(x, Q^2) + Y_- x \mathcal{F}_3(x, Q^2)] , \quad (3)$$

where $Y_\pm = 1 \pm (1 - y)^2$. The parity violating term $x\mathcal{F}_3$ reduces substantially the e^+p cross section. The contribution from F_L is expected to be very small and has been neglected. The dependence on the partonic structure of the proton, and on the Z^0 propagator is absorbed in the positive generalized structure functions \mathcal{F}_2 and \mathcal{F}_3 (see [15] for details on both, the SM predictions and the measurements).

The SM prediction depends on one hand on well measured electroweak parameters as α , the weak mixing angle and M_Z . The errors on their measured values give a negligible uncertainty (at the 0.25% level). The predictions depend also on the quark structure function used. The ZEUS Collaboration uses that from a NLO evolution of parton densities at higher x and lower Q^2 . As a result the u quark dominates the cross section at high x and Q^2 . The uncertainty on the predicted cross section due to the partonic densities is estimated to be at the 6% level.

An example of a very high Q^2 NC candidate can be seen in Fig. 2-left with the e^+ scattered off at large angles. Fig. 6-left-top shows the most up to date ZEUS result for $d\sigma^{\text{NC}}/dQ^2$ at high Q^2 ($Q^2 > 400 \text{ GeV}^2$). We can see how at Q^2 values in the vicinity of M_{Z^0} the $1/Q^4$ dependence of the cross sections is modified as expected from the presence of the Z^0 . The SM prediction follows the data for almost 7 orders of magnitude. For a better comparison, the bottom plot in Fig. 6-left shows the ratio measured/SM expectations for the same Q^2 range. The band shows the uncertainty in the SM prediction coming from the parton density in the proton. There is a little excess at very large Q^2 but its statistical significance is marginal.

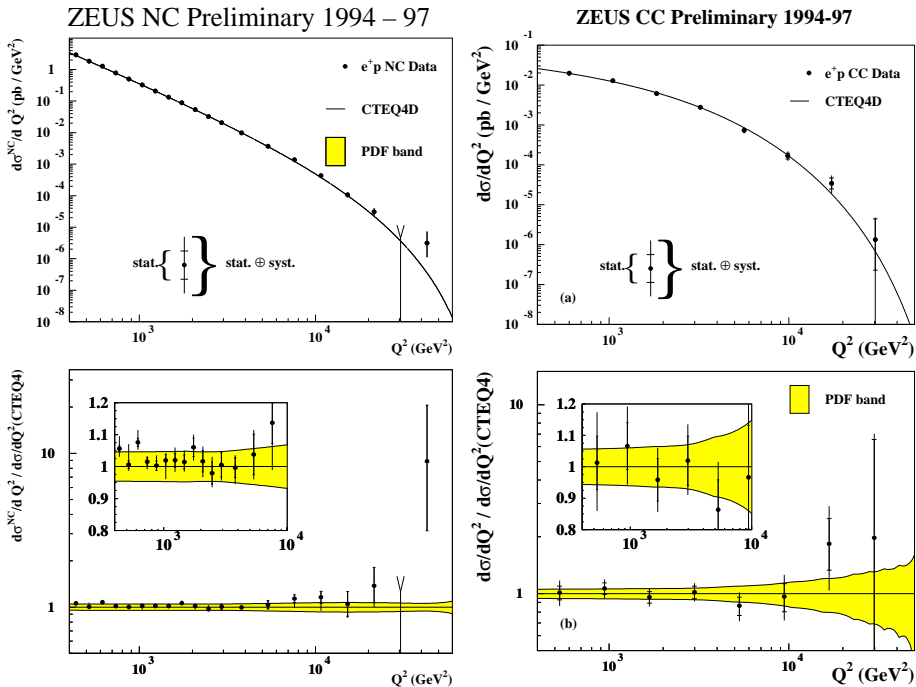


Fig. 6.

In contrast to NC process with the γ and Z^0 as gauge bosons, Charged Current (CC) reactions proceed, within the SM, via the exchange of only the massive W^\pm and therefore their cross sections will be very different. For e^+p scattering ($e^+p \rightarrow \bar{\nu}X$) it is at lowest order

$$\frac{d^2\sigma_{e^+p \rightarrow \bar{\nu}X}}{dx dQ^2} = \frac{G_F^2}{2\pi x} \left(\frac{M_W^2}{M_W^2 + Q^2} \right)^2 \sum_{i=1}^2 [\bar{u}_i(x, Q^2) + (1-y)^2 d_i(x, Q^2)] , \quad (4)$$

where the electroweak part is clearly separated from the dependence on the partonic densities. As the Q^2 dependence of the latter is very mild (of logarithmic type), then, when integrated in x , the Q^2 production cross section will be essentially constant for Q^2 values well below M_W . For Q^2 values of the order of M_W , the W^+ propagator starts acting modifying the Q^2 dependence of the cross section up to the $1/Q^4$ behavior in the limit of very large Q^2 .

One DIS CC candidate can be seen in Fig. 2-right. Its main signature is the large missing transverse momentum. Fig. 6-right-top shows the Q^2 differential cross section for CC DIS measured by ZEUS. The mild Q^2 dependence at low Q^2 is altered in the vicinity of M_W^2 due to the presence of the W^+ propagator. The prediction by the SM follows the measurements for the almost 5 orders of magnitude change in the production cross section. From a fit to the Q^2 dependence of the data a W mass of $M_W = 78.6^{+2.5}_{-2.4}(\text{stat})^{+3.3}_{-3.0}(\text{syst})$ GeV is extracted, in good accord with the results from the Tevatron and LEP.

For the sake of a better data-theory comparison the bottom plot in Fig. 6-right shows the ratio between the cross section measured, and that predicted by the Standard Model. As in the NC case, the data is slightly above the SM prediction at very high Q^2 , although the statistical significance of the discrepancy is even more marginal.

5. Multi jet production at HERA

Multi jet production in HERA final states is a rich field in which the testing of QCD is particularly well suited for. In this talk I will present the latest results by ZEUS on the subject [16].

In the lowest order, two jets in NC DIS are produced via two mechanisms, the so called QCD-compton in which a gluon is radiated from the quark lines, and via the boson gluon fusion (BGF) mechanism which, as its name indicates, can be seen as a γ^*g scattering (see (a) diagram in Fig. 7). The 2-jet cross section at low Q^2 is dominated by BGF.

If we go further down in Q^2 and the exchanged γ is almost real, in addition to the above reactions, the fact that the hadronic component of the γ becomes relevant induces the appearance of new mechanisms, with a parton “within” the photon interacting with a parton in the proton. Those are named as resolved photon reactions. The dominant subprocesses are t-channel gluon exchange diagrams as the one shown by the (b) diagram in Fig. 7. One should notice that in this kind of reactions the lowest order is already at order α_s^2 .

The fact that at very low Q^2 scattering (*i.e.* photoproduction) there occur direct and resolved photon reactions can be investigated “almost directly”

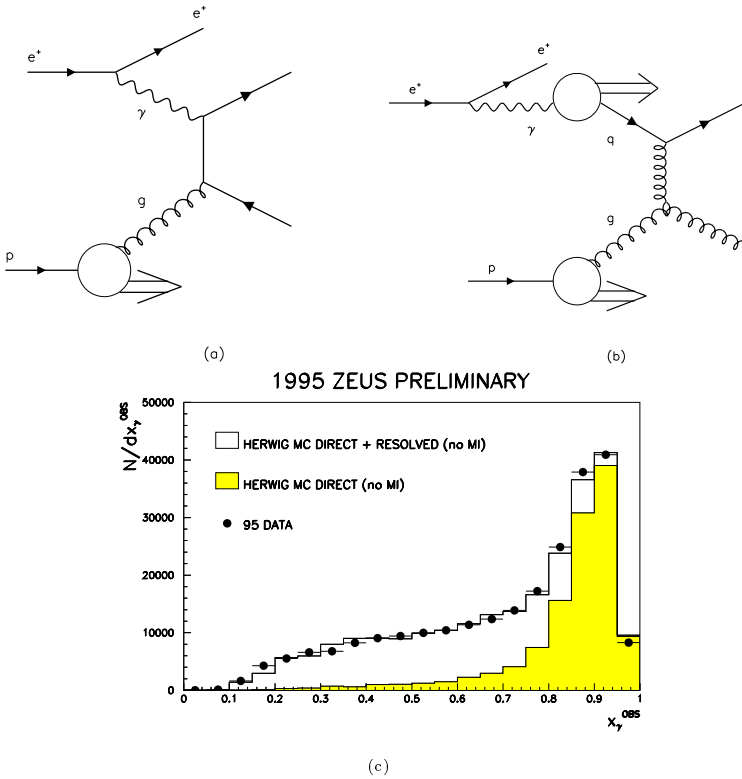


Fig. 7.

by looking at the fraction of the original γ 's momentum which is carried out by the hard interacting initial state parton. This fraction is called x_γ . Obviously for direct reactions $x_\gamma = 1$ whereas for resolved reactions x_γ is smaller than 1. In 2-jet events, x_γ can be determined with the energy and direction of the jets by $x_\gamma^{\text{obs}} = (\sum_{\text{jets}} E_T^{\text{jet}} e^{-\eta^{\text{jet}}}) / (2E_\gamma)$. The resulting distribution is shown in Fig. 7. The data peaks near $x_\gamma = 1$, indicating the predominance of direct reactions, but it shows a large tail extending down to almost $x_\gamma = 0$. This is what one would expect from a substantial resolved component. In fact, if we take a photoproduction Monte Carlo model (MC) with all the LO diagrams, we see in Fig. 7 that it provides a reasonable description of the data. The shadowed histogram is the prediction of this MC for the direct contribution, the rest is resolved.

We may think that this aspect of photoproduction makes life difficult, but as it is a matter of mixing several different 2 to 2 reactions, in reality it is a big advantage if we really want to test QCD. Another big advantage of studying multi jet production at very low Q^2 is that the statistics is

much larger than in the DIS regime. The caveat is that for the predictions, in addition to having to know reasonably well the parton content of the proton we have to know also reasonably well that of the photon. As a result this is not a big problem, since our current limited knowledge induces only small theoretical uncertainties on the predictions for the relevant differential cross sections. QCD calculations at NLO for jet photoproduction have been performed by two groups: Klasen, Kleinwort and Kramer [17] and Harris and Owens [18].

There are several jet search algorithms, the ones used here are the iterative cone and the inclusive k_T . In both cases the search is performed in the pseudorapidity ($\eta = -\ln(\tan(\theta/2))$) azimuth (ϕ) plane in the laboratory frame and using the transverse energy flow of the event (see [16] for details).

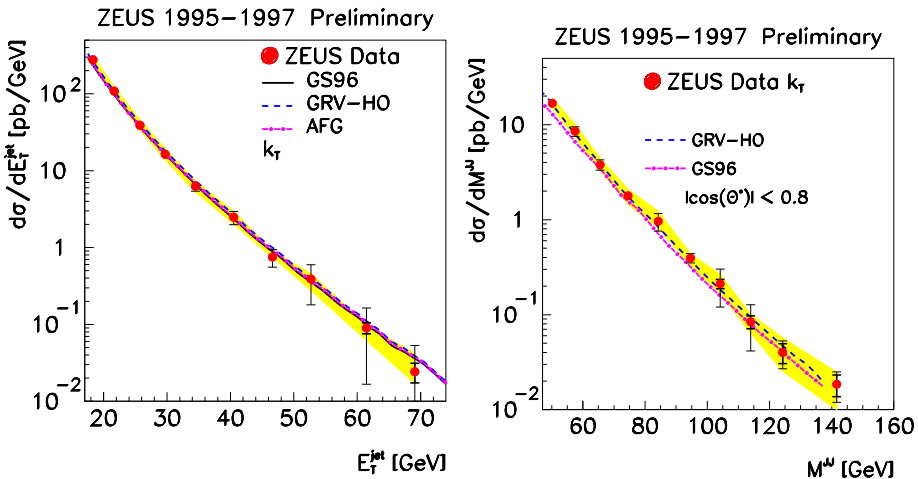


Fig. 8.

Fig. 8-left shows the jet transverse energy differential cross section for inclusive jet production. The data reaches transverse jet energies up to 70 GeV. The band is the uncertainty from the calorimeter energy scale calibration. The NLO calculations, showed for three different parametrizations of the photon's structure function, describe well the data along the 4 orders of magnitude spanned by the cross section.

Fig. 8-right shows the jet-jet invariant mass differential cross section in 2-jet final states. This distribution, in addition to be another test of the QCD predictions, it is sensitive to the presence of new particles or resonances decaying into two jets. The cross section shows an exponential fall off which is in good accord with the NLO calculation excluding the presence of any resonance up to masses of about 150 GeV.

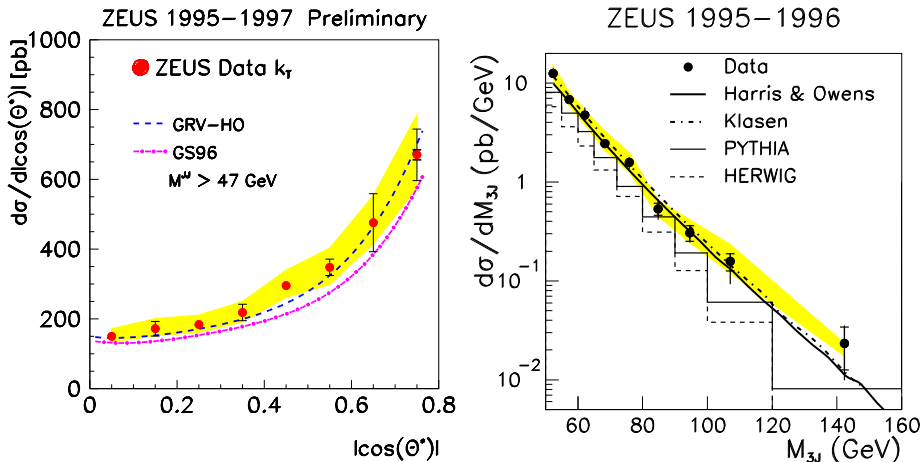


Fig. 9.

Fig. 9-left shows the 2-jet differential cross section as a function of $|\cos(\theta^*)|$. θ^* is the angle between the jet-jet axis and the beam direction in the dijet center-of-mass system. The measured cross section is also well reproduced by NLO QCD. This distribution is sensitive to the photon structure function. The reason for that is its strong dependence on the spin of the propagator (quarks or gluons), which in turn depends on the type of initial state partons in the reaction. Among them, the type of parton coming from the photon depends on partonic content of the latter, *i.e.* the photon structure function.

To end with, Fig. 9-right shows the 3-jet production differential cross section as a function of the invariant mass of the 3-jet system. The NLO calculation gives a satisfactory description of the data. One should notice that this distribution is very sensitive to higher order corrections (at LO there are no 3-jet final states).

6. Charm production at HERA

The main mechanism for charm production at HERA is (at LO) boson gluon fusion in which a charm anti-charm pair is produced in the final state (see Fig. 10-left). Therefore, further testing of QCD can be carried out by contrasting the measured charm production with the recent calculations at NLO by Harris and Smith [19].

In addition, since in the BGF the exchanged γ interacts with a gluon from the proton, we are also probing the gluon content of the latter. This will be an independent measurement to that out of the measurement of the proton's F_2 . I concentrate on charm production in the DIS regime [20].

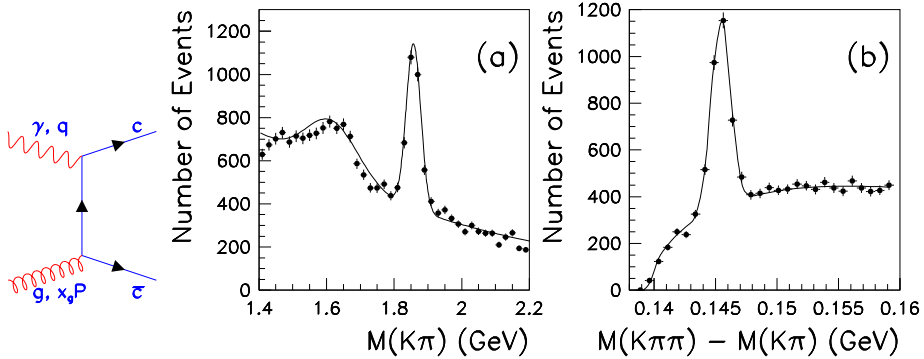


Fig. 10. Preliminary ZEUS 96-97 result

As we, obviously, can not see the charm quark, we instead reconstruct a suited meson containing it. This is the $D^{*\pm}$. The reconstruction is in its decay mode $D^{*+} \rightarrow D^0 \pi_s^+ \rightarrow (K^- \pi^+) \pi_s^+$ (+ c.c.). It has a low branching ratio (2.5%) but produces a very clean D^* signal due to the tight kinematic constraint on the $D^{*+} \rightarrow D^0 \pi_s^+$ decay, which translates into a prominent signal in the distribution of the mass difference between the reconstructed D^* and the reconstructed D^0 .

Tracks from the Central Tracking Detector are assigned to be the K , π and π_s and combined to form the D^* and the D^0 . After applying suited cuts to reduce the combinatorial background the resulting $M(K\pi)$ and $\Delta M = M(K\pi\pi_s) - M(K\pi)$ distributions are shown in Fig. 10-right where clear D^0 and D^* peaks are apparent.

The fully corrected differential cross section for $D^{*\pm}$ production in the kinematic region $1 < Q^2 < 600 \text{ GeV}^2$, $0.02 < y < 0.7$, $1.5 < p_T(D^{*\pm}) < 15 \text{ GeV}$, $|\eta(D^{*\pm})| < 1.5$ (the restriction in $\eta(D^{*\pm})$ corresponds to the active region of the ZEUS central tracking detector) are shown in Fig. 11 as a function of Q^2 , x , W , $p_T(D^*)$, $\eta(D^*)$ and $x(D^*) = 2\bar{p}^*(D^*)/W$. The predictions from NLO QCD are shown as bands which account for our uncertainty in the mass of the charmed quark. They are obtained from the calculated charm production cross sections after proper weighting by the branching ratios and by applying the Peterson fragmentation scheme. The total D^* production cross section measured in the above kinematical region is $\sigma = 8.31 \pm 0.31(\text{stat})_{-0.50}^{+0.30}(\text{syst}) \text{ nb}$ to be compared with the NLO prediction of 8.44 ± 0.55 (the uncertainty comes from that in m_c).

It is interesting to notice the very low values of x in the events. This is expected since the gluons in the proton populate its low x region. Overall, NLO gives a reasonable description of the data. There are though, some discrepancies which are at the edge of being significant. They occur in the

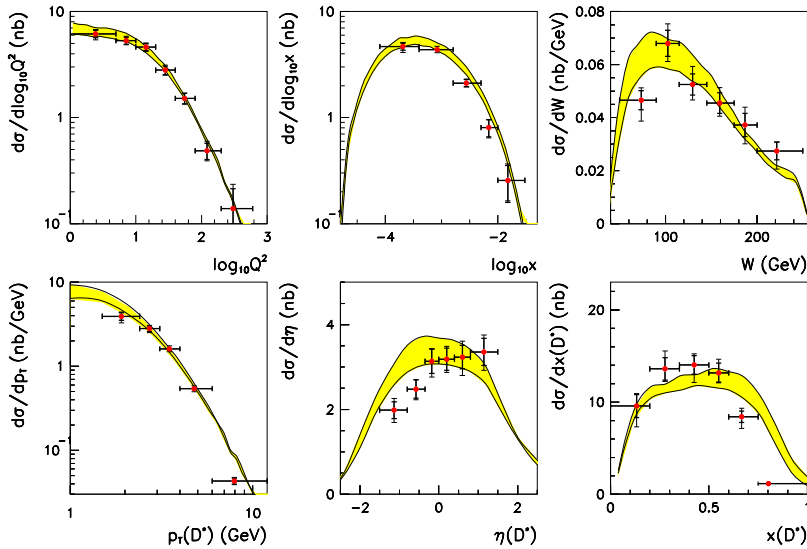


Fig. 11. Preliminary ZEUS 96–97 result

shape of both, the $\eta(D^*)$ and the $x(D^*)$ (the D^* fractional momentum) distributions. These effects, seen also by the H1 Coll. [21], have been understood in terms of the fragmentation of the c quark, which in the HERA environment seem to be by far more complicated than the simple Peterson approach.

We can extrapolate our measured cross sections in the restricted $\eta(D^*)$, $p_T(D^*)$ region to the full region and, by studying the double differential cross section in Q^2 and x , extract the open charm contribution to the proton structure function F_2 . Notice that this would be part of the gluon contribution to the F_2 since the charm is produced, under our approach, by the scattering between the exchanged photon and a gluon within the proton. The result is shown in Fig. 12 where $F_2^{c\bar{c}}$ has been displayed as a function of x for different Q^2 ranges (left) and as a function of Q^2 for different x ranges (right). It shows similar features to those of the full F_2 (see Fig. 3), namely a strong rise with decreasing x which gets milder as we go down in Q^2 and strong scaling violations. The QCD NLO predictions for two NLO proton parametrizations are shown as well in the plots. The agreement theory-measurements is satisfactory.

In order to quantify the open charm contribution to the proton structure function, we show in Fig. 13-left the ratio $F_2^{c\bar{c}}/F_2$ as a function of x for the different Q^2 intervals. It ranges from 10% at low Q^2 values, up to 30% at intermediate Q^2 . It is certainly a sizable contribution but well accounted for by QCD.

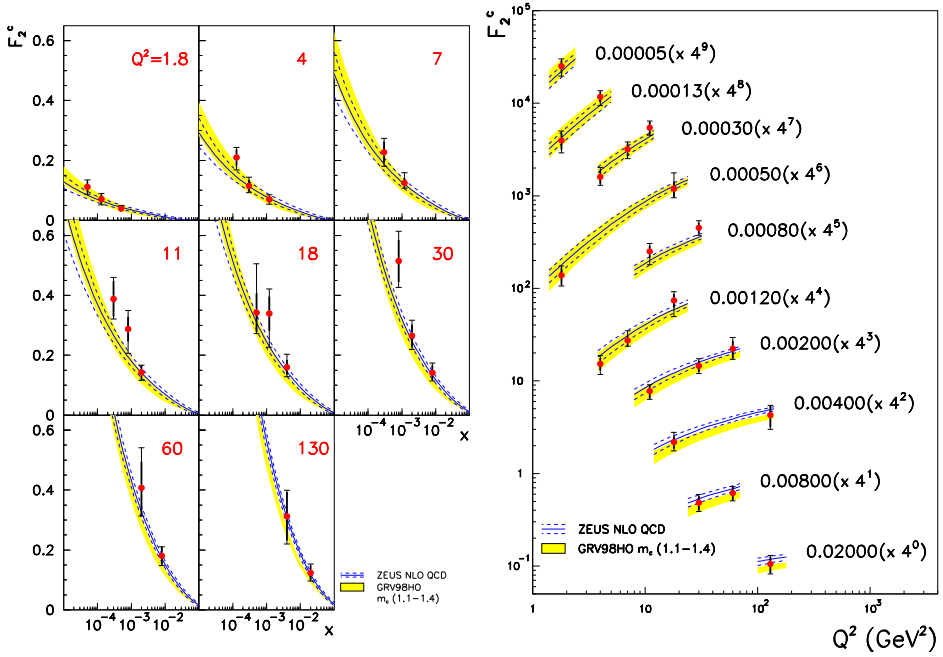


Fig. 12. Preliminary ZEUS 96-97 result

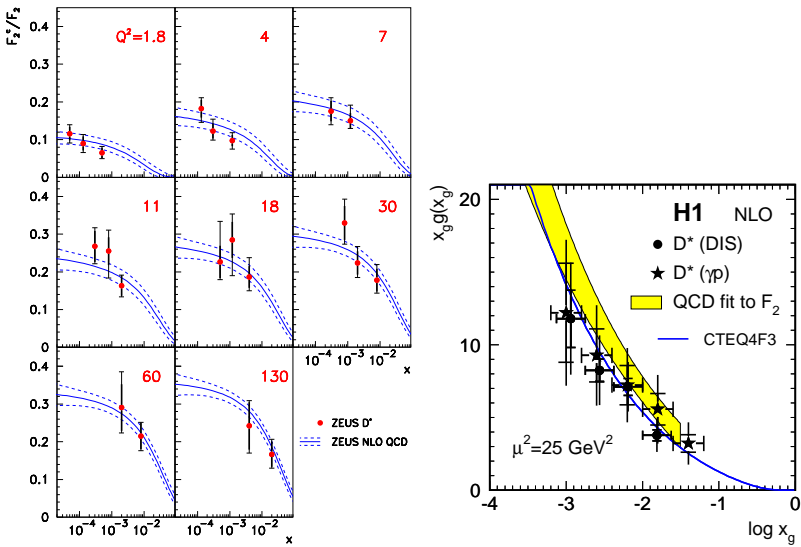


Fig. 13. The result by ZEUS is preliminary

Finally I would like to show an independent measurement of the gluon density in the proton extracted by H1 from the measured kinematics of the scattered e^+ and the D^* (*i.e.* the charm) in the final state. The method is based in the fact that at LO the 2 to 2 process $\gamma g \rightarrow c\bar{c}$ is completely determined if the momenta of one incoming and one outgoing particle (here the γ and the c or \bar{c}) are known (see diagram in Fig. 10). The result is shown in Fig. 13-right. The dots are from the analysis of the D^* production. The band is from the H1 analysis on the F_2 data corresponding to that we have shown from ZEUS. There is a wonderful agreement between both results.

Epilogue

After the analyses presented in this talk I would like to finalize by emphasizing that with HERA our knowledge of the proton is increasing enormously and the strong interaction is being tested exhaustively. Respecting electroweak physics, from the quality and importance of the present results, still low statistics, we foresee a very exciting future with the forthcoming HERA luminosity upgrade.

I would like to warmly thank F. del Aguila and F. Cornet for a superbly organized meeting and for making our stay in Granada so very pleasant. I am indebted to G. Garcia for a careful reading of the manuscript.

REFERENCES

- [1] G. Wolf, HERA Physics, DESY 94-022 (1994).
- [2] A. de Rujula *et al.*, *Phys. Rev.* **D10**, 1649 (1974).
- [3] L.N. Lipatov, *Sov. J. Nucl. Phys.* **23**, 338 (1976).
- [4] ZEUS Coll., M. Derrick *et al.*, *Z. Phys.* **C65**, 379 (1995).
- [5] ZEUS Coll., M. Derrick *et al.*, *Z. Phys.* **C72**, 399 (1996).
- [6] A.D. Martin, W.J. Stirling, R.G. Roberts, *Phys. Rev.* **D50**, 6734 (1994); *Phys. Rev.* **D51**, 4756 (1995).
- [7] M. Glück, E. Reya, A. Vogt, *Z. Phys.* **C53**, 127 (1992); *Phys. Lett.* **B306**, 391 (1993); *Z. Phys.* **C67**, 433 (1995).
- [8] R. Brock *et al.*, *Rev. Mod. Phys.* **67**, 157 (1995).
- [9] V.N. Gribov, L.N. Lipatov, *Sov. J. Nucl. Phys.* **15**, 438 675 (1972); L.N. Lipatov, *Sov. J. Nucl. Phys.* **20**, 95 (1975); Yu.L. Dokshitzer, *Sov. Phys. JETP* **46**, 641 (1977); G. Altarelli, G. Parisi, *Nucl. Phys.* **B126**, 298 (1977).
- [10] A. Donachie, P.V. Landshoff, *Phys. Lett.* **B296**, 227 (1992); *Z. Phys.* **C61**, 139 (1994).
- [11] ZEUS Coll., J.Breitweg *et al.*, *Phys. Lett.* **B407**, 432 (1997).

- [12] ZEUS Coll., J. Breitweg *et al.*, *Eur. Phys. J.* **C7**, 609 (1999).
- [13] K. Adel, F. Barreiro, F.J. Yndurain, *Nucl. Phys.* **B495**, 221 (1997).
- [14] H1 Coll., T. Ahmed *et al.*, *Phys. Lett.* **B324**, 241 (1994).
- [15] ZEUS Coll.; XXIX International Conference on High Energy Physics (ICHEP98); Contributed papers 751, 752; ZEUS Coll., J. Breitweg *et al.*, *Z. Phys.* **C74**, 207 (1997).
- [16] ZEUS Coll.; XXIX International Conference on High Energy Physics (ICHEP98); Contributed papers 805, 810, 812; ZEUS Coll., J. Breitweg *et al.*, *Phys. Lett.* **B443**, 394 (1998).
- [17] M. Klasen, T. Kleinwort, G. Kramer, *Eur. Phys. J.* **C1**, 1 (1998).
- [18] B. Harris, J. Owens, *Phys. Rev.* **D57**, 555 (1995).
- [19] B. Harris, J. Smith, *Phys. Rev.* **D57**, 2806 (1998).
- [20] ZEUS Coll.; XXIX International Conference on High Energy Physics (ICHEP98); Contributed paper 768. I. Redondo for ZEUS Coll.; talk given at the DIS99 conference (Berlin, April 1999).
- [21] H1 Coll., C. Adloff *et al.*, *Nucl. Phys.* **B545**, 21 (1999).